

# The star formation histories of galaxies in the Sloan Digital Sky Survey

Benjamin Panter<sup>1,2</sup>, Raul Jimenez<sup>3</sup>, Alan F. Heavens<sup>2</sup> and Stephane Charlot<sup>1,4</sup>

<sup>1</sup>Max-Planck-Institut für Astrophysik, Karl-Schwarzschild Str. 1, D-85748, Garching bei München, Germany

<sup>2</sup>SUPA \*, Institute for Astronomy, University of Edinburgh, Royal Observatory, Blackford Hill, Edinburgh EH9 3HJ, UK

<sup>3</sup>Dept. of Physics and Astronomy, University of Pennsylvania, Philadelphia, PA 19104, USA

<sup>4</sup>Institut d'Astrophysique de Paris, UMR 7095, 98 bis Boulevard Arago, F-75014 Paris, France

15 August 2018

## ABSTRACT

We present the results of a MOPED analysis of  $\sim 3 \times 10^5$  galaxy spectra from the Sloan Digital Sky Survey Data Release Three (SDSS DR3), with a number of improvements in data, modelling and analysis compared with our previous analysis of DR1. The improvements include: modelling the galaxies with theoretical models at a higher spectral resolution of  $3\text{\AA}$ ; better calibrated data; an extended list of excluded emission lines, and a wider range of dust models. We present new estimates of the cosmic star formation rate, the evolution of stellar mass density and the stellar mass function from the fossil record. In contrast to our earlier work the results show no conclusive peak in the star formation rate out to a redshift around 2 but continue to show conclusive evidence for ‘downsizing’ in the SDSS fossil record. The star formation history is now in good agreement with more traditional instantaneous measures. The galaxy stellar mass function is determined over five decades of mass, and an updated estimate of the current stellar mass density is presented. We also investigate the systematic effects of changes in the stellar population modelling, the spectral resolution, dust modelling, sky lines, spectral resolution and the change of data set. We find that the main changes in the results are due to the improvements in the calibration of the SDSS data, changes in the initial mass function and the theoretical models used.

**Key words:** galaxies: fundamental parameters, galaxies: statistics, galaxies: stellar content

## 1 INTRODUCTION

The quality of spectra of the observed light of unresolved stellar populations has reached enough accuracy that it is possible to make detailed studies of the physical properties of the stellar populations in these galaxies. An excellent example of this new generation of data-sets is given by the Sloan Digital Sky Survey (Gunn et al. 1998; York et al. 2000; Strauss et al. 2002) at low redshift, not only by the size of the spectroscopic sample (about  $10^6$  spectra) but by the quality and wavelength coverage of the spectra. At higher redshift the DEEP2 survey (Davis et al. 2003) is providing a similar database, albeit with a smaller wavelength coverage. Future spectroscopic surveys (e.g. WFMOS) will yield larger samples at even deeper redshifts. Given the quality of the spectra, it is interesting to ask the question of whether reliable information about the stellar population of these galaxies can be inferred from the spectra.

Indeed, several attempts have been made previously to study in detail the physical properties of the SDSS galaxies either by using selected features in the spectra (Kauffmann et al. 2004; Brinchmann et al. 2004; Tremonti et al. 2004) or using the

full spectrum (Panter, Heavens & Jimenez 2003; Heavens et al. 2004; Panter, Heavens, & Jimenez 2004; Cid Fernandes 2005; Mathis et al. 2006; Ocvirk et al. 2006). These studies have led to interesting conclusions about the physical properties of these galaxies. In particular analysis of the SDSS sample (Heavens et al. 2004) and other local galaxies (Thomas et al. 2005) show very clear evidence for ‘downsizing’ - the process by which star formation at low redshift takes place predominantly in low-mass galaxies, whereas more massive galaxies have the bulk of their star-formation activity at high redshift, also observed using other methods. In addition one can also determine the global star formation history in the Universe from this fossil record. Our previous study found broad agreement with observations of contemporary star formation at large lookback times, but suggested that there was a peak in star formation activity at  $z < 1$ . Agreement between the fossil record and contemporary star formation indicators is expected if the Cosmological Principle holds; this expected agreement offers an opportunity in principle to test the assumptions in the modelling of both the fossil record and the instantaneous star formation rates. Of most importance is that both are dependent on the stellar initial mass function, but in different ways, with the instantaneous rates being determined very much by the upper end of the IMF, while the fossil record is determined

\* Scottish Universities Physics Alliance

by a wider range of stars. This offers an opportunity in principle to test the evolution of the IMF as a function of cosmic time.

In our previous work, we have presented results from around  $10^5$  galaxies from the SDSS DR1. This paper enhances the previous results through the introduction of a number of improvements to data and analysis methods, and through an investigation of systematic effects and sensitivity to assumptions. On the data side, we have analysed  $\sim 3 \times 10^5$  galaxies from the SDSS DR3 sample. The extra size of this sample is not particularly important, but the calibration of the data has been improved since DR1. On the methods side, we no longer rebin the data to  $20\text{\AA}$  resolution, but compare the data with a wider range of theoretical models, including the Bruzual & Charlot models (Bruzual & Charlot 2003) at  $3\text{\AA}$  resolution. We consider two stellar initial mass functions (a Salpeter and a Chabrier IMF), and a wider range of dust models. We also make some improvements to the treatment of emission lines, by removing additional weaker lines, since interstellar emission lines are not included in the stellar modelling. Finally, we have also explored the effect of removal of sky lines, using a PCA-based method (Wild & Hewett 2005). These studies give us a reasonable estimate of the sensitivity of the results to the assumptions. As is expected from a sample of this size, changes in the assumptions give rise to much larger variations in the results than the statistical errors. The uncertainties in star formation rates from the stellar models used are typically about a factor of two, which makes it difficult to distinguish between different IMFs, although it may be possible to constrain extreme IMF variations.

The layout of the paper is as follows. In Section 2 we outline the enhancements to the method, and the improvements to the data, and describe the assumptions which are made for analysis of the DR3 sample. In Section 3 we present the new results on star formation history, downsizing and galaxy stellar mass function from the DR3 dataset. We also introduce a method to assess the particular areas where current models are lacking. In Section 4 we show the sensitivity of our results to changes in the assumptions, through analysis of a subset of the data, and in Section 5 we draw conclusions.

Throughout this work we assume a concordance cosmology with  $\Omega_v = 0.73$ ,  $\Omega_m = 0.27$ ,  $H_0 = 71 \text{ kms}^{-1}\text{Mpc}^{-1}$  (Spergel et al. 2003).

## 2 SDSS DR3 ANALYSIS

In this Section we describe briefly the SDSS DR3 dataset, and outline the assumptions in the method, highlighting changes made since the analysis of SDSS DR1 (Heavens et al. 2004).

### 2.1 SDSS DR3 data

The spectrophotometric pipeline used by the SDSS has evolved from the Early Data Release (EDR) to the DR3 sample used here. According to the papers describing each release (Stoughton et al. 2002; Abazajian et al. 2003, 2004, 2005), the pipeline was changed between the EDR, DR1 and DR2 subsets, but remained static between DR2 and DR3. Some DR1 spectra had a slight systematic offset for wavelengths smaller than  $4000\text{\AA}$ . Abazajian et al. (2005) claim that this has been corrected in the DR3. There are no published plans for further improvements. The DR1 data has been re-reduced with the new pipeline and this work considers the set of galaxies contained in the SDSS Main Galaxy Sample (MGS) of

**Table 1.** Regions masked from MOPED fitting.

Wavelength Range ( $\text{\AA}$ )	Reason
3711-3741	[OII]
4087-4117	[SII], H $\delta$
4325-4355	H $\gamma$
4846-4876	H $\beta$
4992-5022	[OIII]
4944-4974	[OIII]
5870-5900	Na
6535-6565	[NII]
6548-6578	H $\alpha$
6569-6599	[NII]
6702-6732	[SII]
6716-6746	[SII]

DR1-3 reduced with the DR2 version of the spectrophotometric pipeline.

We apply further cuts to this main galaxy sample based on those of Shen et al. (2003). Our sample is determined by r band apparent magnitude limits of  $15.0 \leq m_r \leq 17.77$ . The magnitude limits are set by the SDSS target selection criteria, as discussed in Abazajian et al. (2005). The target criteria for surface brightness was  $\mu_r < 24.5$ , although for  $\mu_r > 23.0$  galaxies are included only in certain atmospheric conditions. In order to remove any bias and simplify our  $V_{\text{max}}$  criteria we have cut our sample at  $\mu_r < 23.0$ . At low redshifts a small number of Sloan galaxies are subject to shredding - where a nearby large galaxy is split by the target selection algorithm into several smaller sources. To eliminate this effect, for our star formation analysis we use a range of  $0.01 < z < 0.25$ . This also removes the problems of non Hubble-flow peculiar velocities giving erroneous distances based on redshift, which can have a significant effect on recovered stellar mass. For samples involving a very large redshift range there is a concern that after  $V_{\text{max}}$  weighting an individual galaxy at low redshift can dominate higher redshift galaxy signals. For our criteria we have tested this, and no  $V_{\text{max}}$  weighted galaxy contributes more than a tenth of a percent to the final mass total in each bin. The total number of galaxies in the DR3 Main Galaxy Catalogue is 312415, while the number that satisfy our cuts is 299571. In order to estimate the completeness of the survey we have used the ratio of target galaxies to those which have observed redshifts (P. Nordberg, Priv. Comm.). This does not allow for galaxies which are too close for the targetting algorithm, and we estimate this fraction at a 6% level from the discussion in Strauss et al. (2002). As a result of both these cuts, our effective sky coverage is 2947 square degrees.

We also remove from our analysis a larger set of wavelengths which may be affected by emission lines than in our DR1 analysis. These lines are not modelled by the stellar population codes, which only consider the continuum and absorption features. The excluded restframe wavelength ranges due to emission or emission line filling of features are listed in table 1. We also discount signal with wavelength above  $7800\text{\AA}$  in order to reduce the risk of skyline contamination. Typically the rest frame wavelength range used for analysis is  $3450\text{\AA} - 7800\text{\AA}$ .

## 2.2 Modelling assumptions

### 2.2.1 Stellar population modelling

Both our EDR (Panter, Heavens & Jimenez 2003) and DR1 (Heavens et al. 2004; Panter, Heavens, & Jimenez 2004) studies used the 20 Å resolution models described in Jimenez et al. (2004). The field of stellar population modelling has moved on in the meantime, and models at 3 Å resolution and better are available from various authors. We have used those of Bruzual & Charlot (2003) as the basis for this study.

Although with 20Å models the effect of velocity dispersion can be ignored, there is possibility of significant changes in the input spectrum when working at 3Å. After extensive testing we found that in fact there is very little effect, if any, on the recovered stellar populations and metallicities for a wide range of galaxies. We chose to apply a uniform velocity dispersion of 170 km<sup>-1</sup> to the 3Å models, reflecting a typical value for the Main Galaxy Sample.

### 2.2.2 Initial Mass Functions

Both the instantaneous and fossil approach to star formation determination require assumptions about the Initial Mass Function (IMF). The two methods probe different mass regions and deduce the complete stellar populations by assuming an IMF. For instantaneous measures such as H- $\alpha$  or OII emission the presence of lower mass stars is estimated by working down the mass function from the massive stars which cause the majority of the emission. For high-redshift star formation estimated using the fossil record technique, the contribution to the spectrum from older, less massive stars is used to determine early star formation, requiring extrapolation up the mass function.

In recent years, the choice of IMF has been the subject of much debate - in particular whether a universal IMF can be assumed, both in space and time. Several candidates have been proposed for such a IMF, however single stellar population (SSP) models only include a few. Although disfavoured by observations, the Salpeter IMF (Salpeter 1955) has been used as a reference due to its simplicity; it is a power law. The most recent modification is the Chabrier IMF (Chabrier 2003) which seems to be very successful at reproducing current observations in our galaxy. For the main analysis, we use the Chabrier IMF.

### 2.2.3 Dust

Our previous MOPED studies used a single foreground dust screen. In this parameterisation the strength of the extinction may be characterised by  $E(B - V)$ , and the wavelength dependence of the extinction is determined by the choice of extinction model, which may be empirical or modelled. We used an LMC extinction law for the main analysis, but later we will explore the difference in recovered SFH using the Calzetti (1997) starburst model and the LMC and SMC curves given in Gordon et al. (2003).

We have also computed results using the two-dust parameter model of Charlot & Fall (2000). This is a more physically motivated model of the absorption of starlight by dust, which accounts for the different attenuation affecting young ( $< 10$  Myr) and old stars in galaxies, as characterized by the typical absorption optical depths of dust in giant molecular clouds and in the diffuse ISM. Unfortunately, our investigations have shown that the absorption in giant molecular clouds cannot be well constrained from the optical

continuum emission alone. This dust component would be more tightly constrained by the ultraviolet and infrared continuum emission and by emission-line fluxes. We therefore do not show results based on this model here.

## 2.3 Star formation and metallicity history parametrization

In the past, the SFH of galaxies was typically modelled by an exponential decay with a single parameter - for more complex models one or two bursts of formation were allowed. In fact, it would be better not to put any such constraints on star formation, particularly considering that each galaxy may have (as a result of mergers) several distinctly different aged populations. Star formation takes place in giant molecular clouds, which have a lifetime of around 10<sup>7</sup> years. Splitting the history of the Universe into the lifetimes of these clouds give a natural unit of time for star formation analysis, but unfortunately it would require several thousand of these units to map the age of galaxies formed 13 billion years ago, and the (lack of) sensitivity of the final spectrum to the detailed history would make any estimate of star formation history extremely degenerate. We choose a compromise solution, where we allow 11 time bins in which the star formation rate (SFR) can vary independently. This allows a reasonable time resolution, whilst not being prohibitively slow to compute. For most galaxies this parametrization is a little too ambitious, so we do not recommend the use of the recovered star formation histories on an individual galaxy basis. Extensive testing (Panter, Heavens & Jimenez 2003) shows that for large samples the average star formation history is recovered with good accuracy. Future work will concentrate on recovering only as much detail as the data from an individual galaxy demands. The boundaries between the 11 different bins used are determined by considering bursts of star formation at the beginning and end of each period (at a fixed metallicity) and set the boundaries such that the fractional difference in the final spectrum is the same for each bin. This leads to a set of bins which are almost equally spaced in log(lookback time). Nine bins are spaced with a ratio of log(lookback time) of 2.07 in this application of MOPED, plus a pair of high-redshift bins to improve resolution at  $z > 1$ . This leads to a set of bins whose central ages are 0.0139, 0.0288, 0.0596, 0.123, 0.256, 0.529, 1.01, 2.27, 4.70, 8.50 and 12.0 Gyr. The gas which forms stars in each time bin is also allowed to have a metallicity which can vary independently. The Bruzual & Charlot (2003) models allow metallicities between  $0.02 < (Z/Z_{\odot}) < 1.5$ . In order to investigate metallicity evolution (Panter et al. 2007, in prep) no regularization or other constraint is applied to the metallicity of the populations - each different age can have whatever metallicity fits best. A further complexity to the parametrization to deal with post-merger galaxies which contain gas which has followed dramatically different enrichment processes would be to have several populations with the same age but independent metallicities. It is possible to consider a more complex parametrization, but again one risks degeneracies in solution. With 11 ages, 11 metallicities and the dust parameter, the model has 23 parameters. The 23 dimensional likelihood surface is explored by a Markov Chain Monte Carlo technique outlined in Panter, Heavens & Jimenez (2003) Further information on the MOPED algorithm is contained in Panter (2005).

### 2.3.1 Speed issues

MOPED (Heavens, Jimenez, & Lahav 2000) works by a massive data compression step, forming (in this case) 23 linear combina-

tions of the flux data. The resulting MOPED coefficients are fitted by standard minimum  $\chi^2$  techniques. The data compression step is carefully designed to give answers which are (in ideal circumstances) as accurate as performing a full fit to the  $\sim 3852$  flux data. One of the benefits of the MOPED algorithm is that the number of compressed data is determined by the number of model parameters, not the number of data points. This has the huge advantage that analysis of the spectra at  $3\text{\AA}$  resolution is no slower than analysis of  $20\text{\AA}$  spectra (except for a small increase in overheads such as pre-computing the data compression weighting vectors). The algorithm takes around two minutes per galaxy on a fast desktop workstation, and represents a speed up of around a factor of 170 over a brute-force likelihood fit.

## 2.4 Computing Ensemble Results

### 2.4.1 Common star formation time bins

MOPED determines the star formation history of each galaxy, relative to the lookback time. To obtain the cosmic SFR it is necessary to shift these results to a common set of time bins, which for simplicity are chosen to be the same as those used in the galaxy analysis. This allows direct comparison of galaxy star formation between galaxies at different redshifts in terms of cosmic time, and ensemble conclusions to be drawn. The shifting algorithm ensures conservation of star formation. Star formation in the oldest bin is always assigned to the final bin with ages no greater than 13.7 Gyr, the age of the Universe determined by the concordant WMAP cosmology.

### 2.4.2 Inverse $V_{\max}$ weighting for Fossil studies

In a magnitude-limited survey such as the SDSS the range of galaxy types and sizes included in the survey will vary over the redshift range studied. Some mechanism is required to compensate for this change and determine the overall bulk parameters for the sample. To convert from star formation rates to star formation rate density, galaxies are weighted by  $1/V_{\max}$ , where  $V_{\max}$  is the maximum volume of the survey in which the galaxy could be observed in the SDSS sample. This gives an unbiased estimate of the space density  $f$  of any additive property  $F$  of the galaxy under investigation, such as mass, luminosity, star formation rate.

$$f = \sum_{\text{galaxies } i} \frac{F_i}{V_{\max,i}} \quad (1)$$

On smaller scales the estimator is affected by source clustering, but the SDSS is deep enough that these variations should not be significant. Any properties which change with redshift and which could determine inclusion in the sample must be calculated for each galaxy over the redshift range of the survey to determine whether or not it would have been included. In order to calculate the  $V_{\max}$  assigned to each galaxy it is necessary to consider the apparent magnitude and surface brightness evolution over the redshift range. In order to compute this we use the same stellar evolution models used in the MOPED analysis to calculate luminosity over the lifetime of the galaxy due to its recovered star formation history.

The magnitude of a galaxy over its lifetime depends on the luminosity behaviour of the various stellar populations that make it up - the star formation history. As young stars, the populations will have a very high light output, which will reduce as they age. This information is encoded in the galaxy spectrum and recovered by

MOPED, which gives the relative fractions of different aged populations. To compute the observed magnitude if the galaxy were to be observed at higher redshifts, we need to evolve the models over time and track the changes in luminosity. Obviously, as the galaxy is projected to a further redshift the younger fractions do not contribute, as galaxy is being ‘observed’ before these populations were born. Since the spectral energy distribution of the light changes with evolution of the galaxy, it is also necessary to apply the filters used by Sloan to determine the flux included in the  $r$  band, leading to a change in  $c_{i,z}$  in the  $r$ -band magnitude as the redshift is changed:

$$r_{i,z} = r_{i,z_{\text{obs}}} + c_{i,z}. \quad (2)$$

These magnitude corrections can then be used to calculate corrections which need to be applied to the surface brightness. The surface brightness of the galaxy at each redshift  $z$  is

$$\mu_{i,z} = r_{i,z} + c_{i,z} + 2.5 \log_{10} [\pi r_{50,i}^2 (D_z/D_{z_{\text{obs}}})^2] + 2.5 \log_{10} 2 \quad (3)$$

where  $D_z$  is the luminosity distance,  $r_{50}$  is the Petrosian half light radius and  $z_{\text{obs}}$  is the observed redshift of the galaxy. This equation assumes that the size of the galaxy does not change over the redshift range. Although this assumption is valid for low redshift sources, it will need to be developed if the technique is applied to deeper surveys.

The MOPED technique gives the relative strengths of the different spectral models. The mass originally created to make these masses is then calculated, and by dividing this by the maximum volume over which the galaxy could be observed gives the star forming density,  $\rho_i$ . By adding all the  $V_{\max}^{-1}$  weighted star forming densities of galaxies in the sample, rebinned to a common time frame, the overall star forming density  $\rho$  can be found for the region studied.

Galaxies may only contribute to the SFR of a time bin if they are at a lower redshift than the lower limit of that bin. This conservative approach ensures that the star formation of a galaxy is never extrapolated. It also means that in all but a few cases where a galaxy is almost on the boundary between bins, the youngest populations, those which are better calculated using instantaneous indicators from emission lines, do not contribute to estimates of the SFR. In addition, to ensure that our results are not biased by single erroneous SFH reconstructions we only present results from bins which contain contributions from greater than 1000 galaxies.

## 3 RESULTS FROM THE DR3

### 3.1 Evolution of Stellar Mass Density

The simplest interpretation of the combined star formation histories is a simple  $V_{\max}^{-1}$  weighted addition that shows how the present day stellar mass of the Universe has built up. In Fig. 1 and Table 2 we show how the stellar mass density of the universe has changed since  $z = 2$ . In order to compute the remaining mass (when from the MOPED algorithm we estimate the original mass of stars formed) it is necessary to invoke the recycling fraction,  $R$ . Rather than assume a blanket correction, we have used the detailed predictions allowed by the Bruzual & Charlot (2003) models for each population of each galaxy, based on their determined ages and metallicities. Although this is slightly more laborious than assuming a blanket recycling fraction it gives a more accurate determination of present mass, since  $R$  is a function of both age and metallicity.

The abscissa on this plot refers to the minimum redshift of a

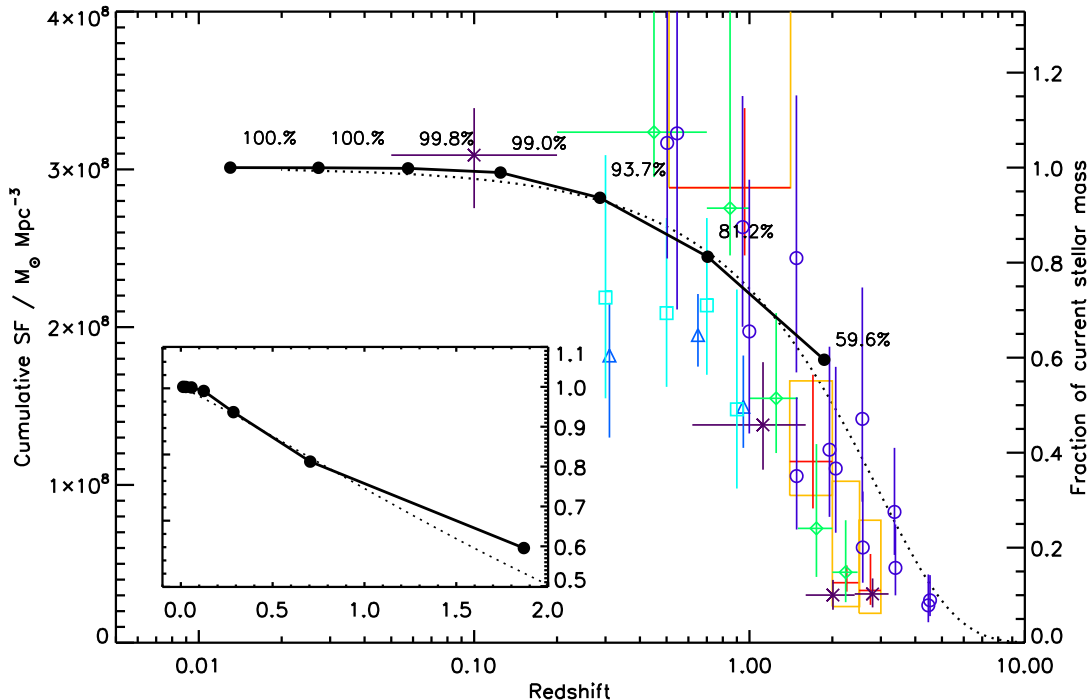


**Figure 1.** The build up of the current stellar mass density of the Universe, as determined from the SDSS DR3 galaxies and the recycling fractions from the Bruzual & Charlot (2003) models with appropriate  $V_{\text{max}}^{-1}$  weights (heavy dots, solid line). In all cases statistical errors are contained within the dots marking the actual data points. Also plotted for comparison are estimates from other surveys: HDF-N, Dickinson et al. (2003) (red plus, orange box denotes their error estimation), HDF-S, Rudnick et al. (2003) (purple stars), HST/CFRS, Brinchmann & Ellis (2000) (blue triangles), K20, Fontana et al. (2004) (green diamonds), FORS Deep and GOODS-South Fields, Drory et al. (2005) (hollow blue circles). For comparison with simulations we also show the semi-analytical results based on the Millennium Simulation of Croton et al. (2006) (dotted line), normalised to our own final stellar mass density. Insert shows exactly the same data plotted on a linear redshift axis. No attempt has been made to convert between assumed initial mass functions.

**Table 2.** The buildup of stellar density derived from the MOPED/SDSS-DR3 fossil record.

$z$	Stellar Mass Density	Min Density $\log_{10}(M_{\odot} \text{Mpc}^{-3})$	Max Density
0.0130	8.459	8.401	8.558
0.0272	8.459	8.401	8.557
0.0575	8.458	8.401	8.556
0.125	8.454	8.399	8.549
0.286	8.427	8.377	8.516
0.705	8.362	8.317	8.447
1.87	8.222	8.186	8.309

given bin, when all the stars formed in that bin will be in place. Simple interpolation between these points is valid as long as the star formation rate is constant across the bin. From this it is easy to see that approximately 60% of the present day stellar mass was in place by  $z = 1$ , and 90% by  $z = 0.35$ . It is also clear that in our sample there is overall very little star formation at  $z < 0.1$ .

For comparison we also plot the mass buildup estimated from various surveys. We also show the results from semi-analytical modelling based on the Millennium Simulation (Croton et al. 2006). The data shows excellent agreement between the largest astronomical survey and the largest simulation ever undertaken. The statistical errors on the points in Fig. 1 are so small that they are con-

tained within the points. This is of course unrealistic, and we have also included a more realistic treatment of errors in our ensemble estimates by selecting many different (but still reasonable) sample criteria and comparing the ensemble results that result from each sample. These separate samples vary between minimum redshift (0.001, 0.003, 0.006, 0.009, 0.01, 0.03, 0.05), maximum redshift (0.2, 0.3, 0.34), bright limiting magnitude (13.5, 14.0, 14.5, 15.0), faint limiting magnitude (17.7, 17.77) and surface brightness cuts (23.0, 23.5, 24.0). They show the maximum and minimum recovered quantities from the many ways of selecting source galaxies, and should be indicative of the systematic errors from basing the analysis on different galaxies, although some of this variation will come from real differences between the histories of the galaxies selected. The extents of these systematic (and heavily correlated) error approximations are not plotted, but are given in Table 2 as maximum and minimum densities. In the case of the cumulative stellar mass density the overall mass can vary by up to 25%.

### 3.2 The cosmic star formation rate

In Fig. 2 we show the cosmic star formation recovered from SDSS DR3 with a Chabrier initial mass function, using the Bruzual & Charlot (2003)  $3\text{\AA}$  resolution spectral synthesis models, and a single-parameter dust screen following the extinction curve of the LMC.

As seen before in many studies, the steep decline in SFR is clearly demonstrated. In contrast to our previous study, we do not

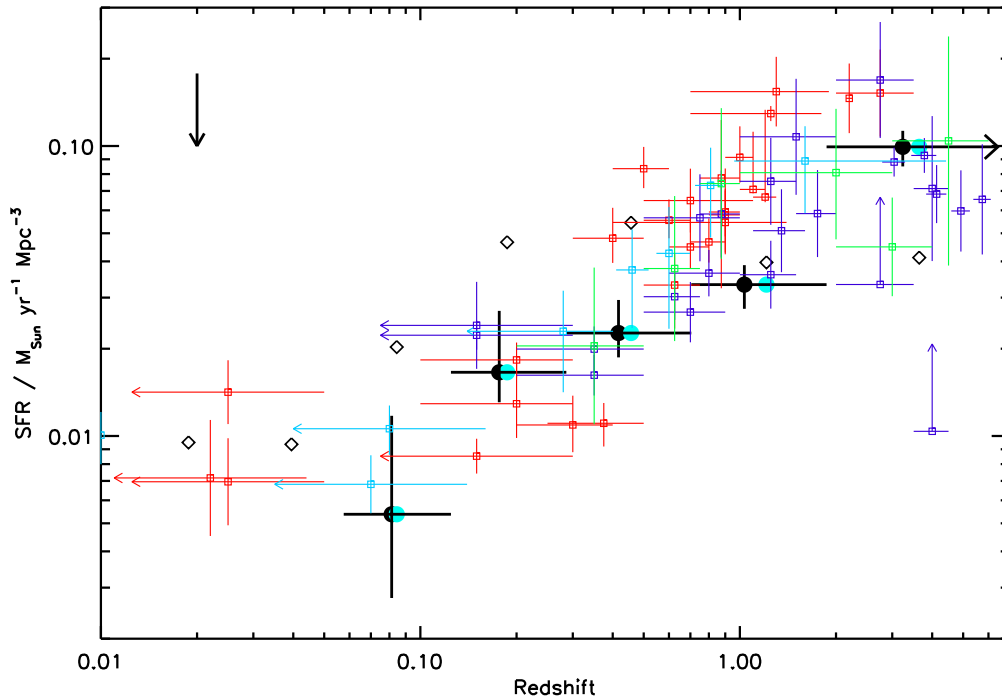


**Figure 2.** The cosmic star formation history of the Universe, as determined from the SDSS DR3 galaxies (heavy black horizontal bars cover the bins, the luminosity weighted age of each bin given by black dots). The vertical error bars are indicative of systematic errors arising from choosing different subsets of the data for analysis. See text for full details. Also plotted for comparison are the estimates from our DR1 work (black diamonds) (Heavens et al. 2004) and those compiled in Hopkins (2004), using the common obscuration discussed within that paper. The points have also been corrected for the minor difference in cosmology between that work and this paper, and shifted downwards by 0.25 dex to convert from the Salpeter to Chabrier IMF as indicated by the arrow in the top left. The Hopkins (2004) points are coded as follows: UV indicators (dark blue): Giavalisco et al. (2004); Wilson et al. (2002); Massarotti et al. (2001); Sullivan et al. (2000); Steidel et al. (1999); Cowie et al. (1999); Treyer et al. (1998); Connolly et al. (1997); Lilly et al. (1996); Madau et al. (1996); OII, H- $\alpha$  and H- $\beta$  emission (red): Teplitz et al. (2003); Gallego et al. (2002); Hogg et al. (1998); Hammer et al. (1997); Pettini et al. (1998); Pérez-González et al. (2003); Tresse et al. (2002); Moorwood et al. (2000); Hopkins et al. (2000); Sullivan et al. (2000); Glazebrook et al. (1999); (1999); Tresse & Maddox (1998); Gallego et al. (1995); sub-mm (green) Flores et al (1999); Barger et al. (2000); Hughes et al. (1998); x-ray and radio (light blue): Condon et al. (2002); Sadler et al. (2002); Serjeant et al. (2002); Machalski & Godlowski (2000); Haarsma et al. (2000); Condon (1989); Georgakakis et al. (2003).

find a peak in SFR at  $z < 1$ . This was also found by Mathis et al. (2006), in work based on the MOPED fossil analysis approach. If there is a peak, it occurs somewhere in our last bin ( $z \gtrsim 2$ ). These new results from the fossil record are in much better agreement with determinations based on contemporary star formation rates. Purely statistical error bars are so small to be almost invisible in all but the lowest redshift bin. As with the previous figure, the vertical error bars in Fig. 2 are indicative only. They show the maximum and minimum recovered star formation rates from the many ways of selecting source galaxies. They should be indicative of the systematic errors from basing the analysis on different galaxies, although some of this variation will come from real differences between the histories of the galaxies selected.

Although for completeness we show our results from  $z \sim 0.1$ , we do not present points with  $z \ll 0.1$  for three reasons. First, from Fig. 1 it is clear that there is much less mass in these bins on which to form an estimate of the SFR, the change in mass with time. Second, to avoid biasing, our  $V_{\max}$  criteria exclude galaxies from contributing to bins with upper boundary lower than their redshift - hence the bulk of the galaxies, at approximately  $z = 0.1$ , can only contribute to bins from  $z = 0.2$  onwards. Third, the galaxies contained in these bins, and the resultant SFR, are strongly dependent on sample criteria, as expected when sample size drops.

**Table 3.** The SFR density derived from the MOPED/SDSS-DR3 fossil record.

$z$	$z_{min}$	$z_{max}$	SFRd	Min SFRd ( $M_{\odot} \text{yr}^{-1} \text{Mpc}^{-3}$ )	Max SFRd
0.081	0.0575	0.125	0.00537	0.00276	0.0117
0.177	0.125	0.286	0.0166	0.0131	0.0270
0.416	0.286	0.705	0.0226	0.0187	0.0294
1.03	0.705	1.87	0.0332	0.0275	0.0388
3.24	1.87	6.42	0.0993	0.0850	0.113

Later in this paper we analyse a subset of the data to determine which changes are responsible for the modifications to the results; the main reasons for the changes are the better calibration of the SDSS DR3, the change in IMF to Chabrier (2003) and the change to the higher-resolution Bruzual and Charlot (2003) models. The star formation rate density resulting from the MOPED DR3 analysis is presented in table 3.

### 3.3 The mass function of stellar mass and $\Omega_{b*}$

The galaxy stellar mass function of SDSS DR3 is shown in Fig. 3, for a range of almost 5 decades in mass ( $10^7 - 10^{12} M_{\odot}$ ). The errors shown are statistical based on our chosen sample criteria. We also compute the mass function for the alternative sample criteria to develop systematic errors. Over much of this range a Schechter fit is good, with parameters  $\phi^* = (2.2 \pm 0.5_{stat} \pm 1_{sys}) \times 10^{-3} \text{ Mpc}^{-3}$ ,  $M^* = (1.005 \pm 0.004_{stat} \pm 0.200_{sys}) \times 10^{11} M_{\odot}$ , and slope  $\alpha = -1.222 \pm 0.002_{stat} \pm 0.1_{sys}$  calculated in the region where there are more than 300 galaxies contributing to each bin ( $10^{8.5} - 10^{11.85} M_{\odot}$ ). The mass function is very similar to our DR1 analysis (Panter, Heavens, & Jimenez 2004), but shifted to lower masses as a result of the use of the Chabrier IMF rather than Salpeter. For further discussion of the systematic differences in recovered galaxy mass caused by IMF variation refer to the discussion in Bell & de Jong (2001).

The stellar mass function can be used to give a further constraint on the contribution to the density parameter from baryons in stars,  $\Omega_{b*}$ . By integrating the mass over the range of the mass function we deduce a value of  $\Omega_{b*} = (1.82 \pm 0.03_{stat} \pm 0.1_{sys}) \times 10^{-3}$  (systematic error). This value is in broad agreement with results obtained previously when the correction from Salpeter IMF is taken into account (Panter, Heavens, & Jimenez 2004; Cole et al. 2001; Bell et al. 2003; Fukugita et al. 1998; Kochanek et al. 2001; Glazebrook et al. 2003; Persic et al. 1992; Salucci et al. 1999). The statistical errors reflect the spread of results obtained with varying sample criteria as before.

### 3.4 Downsizing

One of the results of Heavens et al. (2004) was the finding of ‘downsizing’ from the SDSS fossil record. Using the new models at higher resolution we have found that the evidence for downsizing is just as clear. In Fig. 4 we show the cosmic star formation rate for galaxies split into different stellar mass ranges. A clear signature of ‘downsizing’ is seen: the stars ending up in today’s highest-mass galaxies formed early, and show negligible recent star formation, while the lower-mass galaxies continue with star formation until the present day. The lower, non-offset plot can be used to determine for a given redshift which galaxies dominate the star formation rate.

### 3.5 Investigating spectral residuals

Due to the power of MOPED and the number of SSPs offered for fitting (11) excellent fits can be obtained if the models are accurate. By comparing the residuals of the best fitting spectrum to the raw data on a pixel by pixel basis and then averaging over many galaxies *in the galaxy restframe* it is possible to determine exactly which areas are not being accurately fitted for a given spectrum. By stacking the residuals of high signal to noise (Sloan SPECJOBALL.SCLSN, science  $S/N > 20$  per flux measurement) galaxies it is possible to determine to a high degree of accuracy which wavelength ranges are failing in the models, and to what extent. If we assume that MOPED can, in most cases, obtain the best possible fit to a spectrum then the differences must be features not included in the models. These features could be things that the models are not designed to measure (instrumental effects, interstellar or intergalactic medium absorption, skyline contamination etc.) or alternatively features that are either misrepresented or not yet included in stellar modelling codes (e.g. alpha enhancement

(Thomas, Maraston, & Bender 2003), emission lines, helium production of  $dY/dZ \sim 1.5 - 2$  (Jimenez et al. 2003) and other spectral features). Fig 5 provides some insight into which features in the residuals can be identified. Since we subtract the modelled spectrum from the data, unfitted emission will have a positive effect on the residuals while unfitted absorption will be negative. Both obvious emission lines and filling of absorption features should be detectable. The spectra used for this analysis are those which have already had the strongest emission line regions removed, as detailed earlier - in this case the residual is simply zero.

The first panel of Fig. 5 shows the mean spectrum. To distinguish between galaxy features and skyline features we select two redshift ranges with the same central redshift,  $z = 0.1$ . Since the averaging of residuals is carried out in the galaxy restframe, increasing the redshift spread will act to spread any skyline features. The third panel gives the residuals for galaxies within 0.001 of the central redshift while the second has a range of 0.01. The fourth panel shows the second subtracted from the first. In this case, skyline/instrumental will create regions with large amplitude. The relevant skyline features (and their convolutions with the extremes of the particular redshift distribution) are shown and correspond exactly. It can be seen from the third panel that the majority of the spectral range is remarkably clear of skyline contamination - testament to the high quality of the Sloan spectroscopy.

Considering the regions which are not excluded by skylines we begin to be able to assess the ability of the Bruzual & Charlot (2003) models to fit the data. It is clear that in all regions where weak emission filling could be present and has not been masked there is a slight positive tendency in the residuals (although this is of course not a failing of the models but a reflection of possible systematics affecting our fits), and many of the features in the residual correspond to features that may be affected by alpha enhancement. A more detailed study of individual indices and their alpha enhancement, and their resolution in more advanced models including variable abundance ratios will be presented in a later paper. Although the vast majority of features in the residual can be directly related to specific lines there is a strong signal just red of the magnesium line at restframe 5176Å. Although tempting to attribute this to poor fitting of the magnesium feature, it could also be interpreted as part of a broader feature between restframe 5200-5900Å. It is interesting to compare the fitting in this region to the area around the 4000Å break as both are heavily dependent on metallicity. It is surprising that the models do so well in fitting the break but cannot simultaneously fit this region, and taken with the excess around the Calcium Hydride band (6830-6900Å) suggest that perhaps the balance of K-M giants in the models must be improved, the resolution of which would lead to a bluer continuum.

Converting this feature to the observed frame it coincides with the dichroic region of the combined red and blue SDSS spectrographs. If this were to be the cause one would expect that the feature would appear in the third panel, which it does not, and certainly further work would be necessary to interpret this residual feature in the context of the DR3 spectrophotometric calibration pipeline.

## 4 THE IMPACT OF MODEL CHOICE

In this section, we investigate the influence on assumptions on the results obtained in the last section. There have been several improvements and changes since our analysis of DR1, and the results have changed to some degree. The purpose of this study is to see how the assumptions change the conclusions, and to get some idea

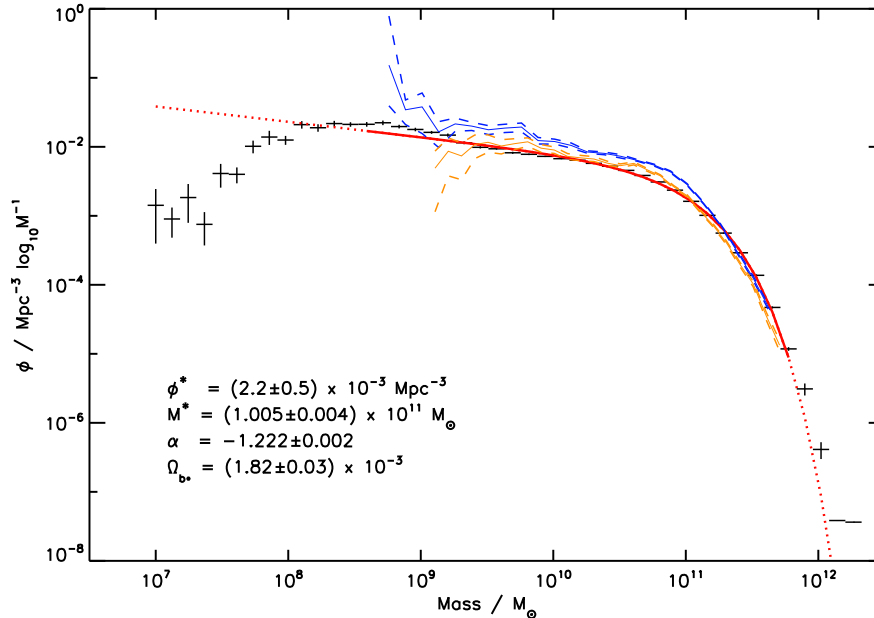


**Figure 3.** The galaxy stellar mass function of SDSS. Also shown are those of Cole et al. (2001) (Orange) and Bell et al. (2003) (Blue), corrected for differences in IMF. The errors quoted on the parameters are based upon the statistical errors of the galaxy sample rather than systematics, which are discussed in the text. The red solid line is the Schechter (1976) best fit solution over the qualifying points, the dotted section is an extrapolation over the range covered by the data.

of the systematic effects introduced by choices of such things as the stellar populations used to model the spectra.

#### 4.1 Sample studied

Although the MOPED algorithm allows rapid analysis of different modelling choices, to investigate a wide range of parameters it is necessary to cut the sample down to something more manageable. We chose to operate on the main galaxy sample spectra in plates 0288 and 0444. These two plates form a representative sample of 808 galaxies from two widely separated patches on the sky. In total 767 of the 808 satisfy the criteria used in our main analysis and would appear in our estimates of SFR.

#### 4.2 Star Formation Fractions and Star Formation Rates

There are two places where modelling choices affect the shape of the recovered cosmic star formation rate - the estimation of the relative fractions of different SSPs and the calculation of a  $V_{\max}$  correction based on that SFH. For this analysis we wish to investigate the two stages independently. To achieve this we need to compare both the SFF recovered using different models and the SFR that results.

The galaxies' star formation fractions (SFF) and total mass are calculated in their individual rest frames. This SFH is then converted to a common frame for all galaxies and weighted in proportion to  $1/V_{\max}$ . Both the original SFF and the  $1/V_{\max}$  weighting are calculated by the models, and the mass is dependent on the IMF. Our first comparison (Fig. 6) shows the initial normalized SFF recovered for the galaxies *averaged in their restframes*. Since it is our intention to compare the relative fractions produced by changing model parameters rather than the overall mass (which has been described elsewhere, see Bell & de Jong (2001)) we present the SFF normalized to total star formation of 1 per galaxy. This should

**Table 4.** A summary of models used in the analysis.

Name	Reference	FWHM
SPEED	Jimenez et al. (2004)	20Å
PEGASE	Fioc & Rocca-Volmerange (1997)	20Å
BC93	Bruzual & Charlot (1993)	20Å
Maraston	Maraston (2005)	20Å
GALAXEV	Bruzual & Charlot (2003)	3Å

give a clear indication of differences on recovered star formation fractions in the models.

Next we compare the cosmic SFR calculated using these various modelling choices. This method allows direct comparison of the SFR obtained using each model, but is subject to greater errors due to the sensitivity of the  $V_{\max}$  calculation on individual star formation histories and the large relative weight change this can produce. We present this model-dependent SFR in addition to the SFF but caution that the number of galaxies present is insufficient to draw robust conclusions. Given the substantially smaller number of galaxies, the errors are far larger than those of the complete DR3 analysis presented earlier in this paper.

A summary of the models is given in table 4; unless otherwise stated a Salpeter (1955) IMF is used to calculate the SSPs.

#### 4.3 Sample galaxies compared to full dataset

Fig 6a shows the difference in recovered SFF between our original DR1 analysis and our subsample. The differences are due to the number of galaxies (120,000 in the full DR1 vs. 808 in the DR1 Sample). For all further comparisons in this section the sample of galaxies will be 808 identified in the MGS plates 0288 and 0444. Fig 8a shows the difference in SFR.



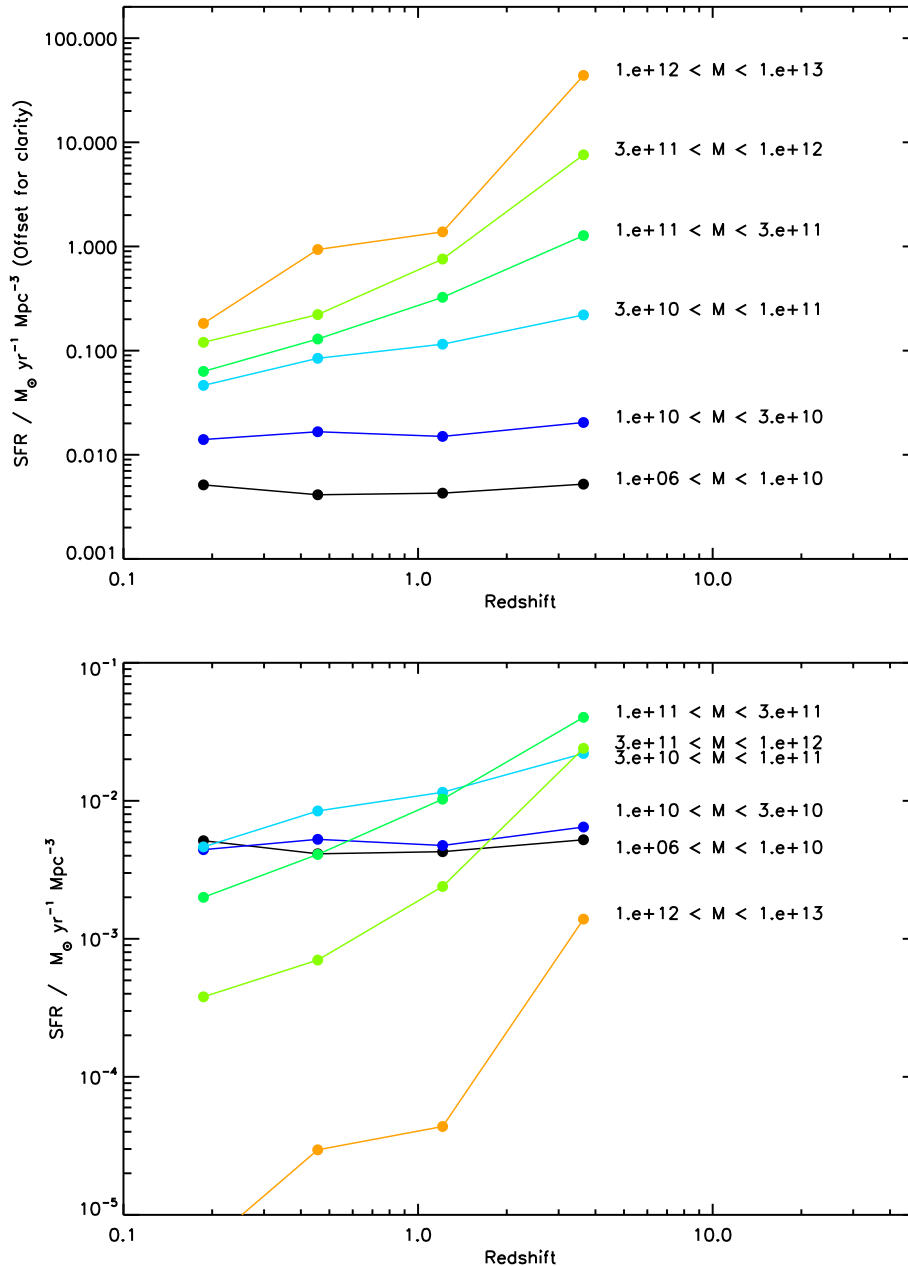


**Figure 4.** The star formation rate of galaxies of different masses. These plots show the contribution to the overall star formation rate in the universe from galaxies with different masses over the redshift range we consider reliable. In the upper panel the SFR has been offset to enable easier comparison of the curves, in the lower there has been no offset applied. It is clear that the more massive systems formed their stars earlier, although no conclusion can be drawn as to the number of objects these stars formed in.

#### 4.4 Pipeline changes DR3 vs DR1, PCA cleaning of skylines

Fig 6b shows the impact of changing the pipeline used to reduce the original raw data. DR3 contains a more accurate calibration of the continuum of the spectrum and a systematic trend that deviated the continuum blueward of 4000 Å has been corrected. The SPEED model, at a resolution of 20Å was used for all three sets. Except for bins 6-9 (numbered from the right), the variation the two datasets introduce is very small, at the few percent level. However, for these bins the deviations are as much as a factor of three. Note that, where present, continuum discrepancies between the blue end

for DR1 and DR3 were on average 10% in the flux (at 3500 Å). It is remarkable that such drastic changes introduce such small changes on the average physical properties of the sample.

It is reassuring that the changes made to the spectra by PCA removal of skyline regions have virtually no effect on our SSP fits. It is important to realise though that the majority of the regions cleaned by the Wild & Hewett (2005) code are outside of our sampled wavelength range.

The effect of the pipeline on the SFR shown in Fig 8b is far greater. The mean flux of the spectra between the two releases has changed by a factor of between 1.5 and 2, and the masses reflect



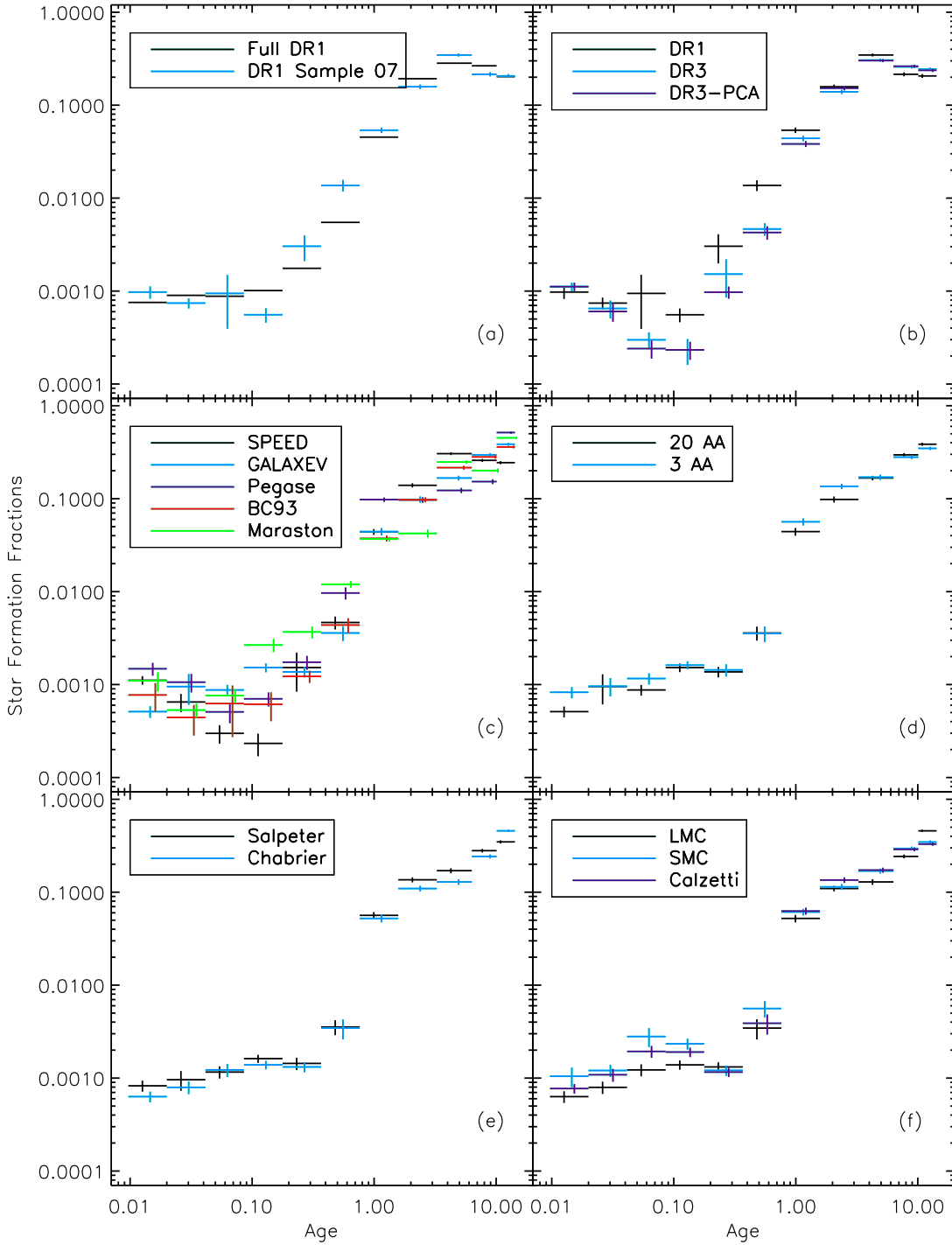


**Figure 6.** The systematic changes in recovered SFH for various modelling choices. The labels show the various modelling choices applied to generate the SFFs, and are expanded upon in the text. It is important to note that these are the fractions of total mass formed over the lifetime of the galaxy, and not the fractions of light contributing to the recovered spectrum. The light from the youngest populations is some 300x brighter than the oldest. The fractions are normalised, so changes in overall recovered mass for spectra are not apparent.

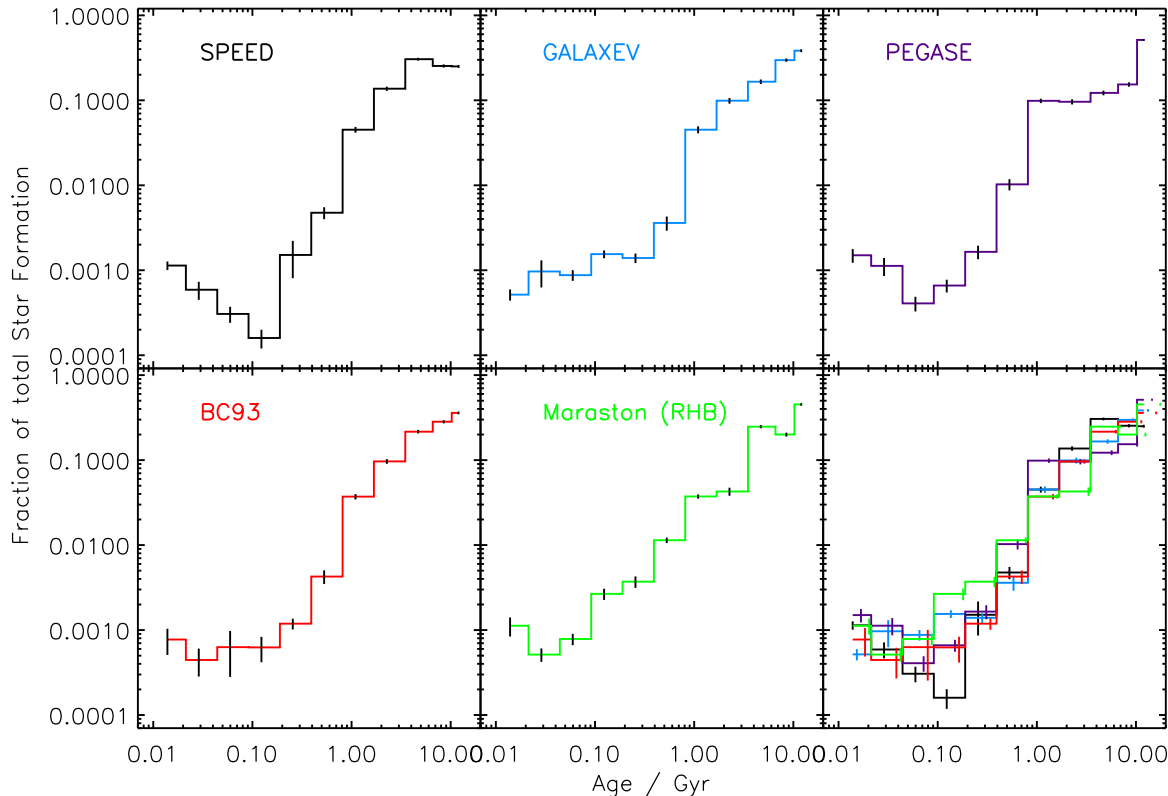


**Figure 7.** The systematic changes in recovered rest frame star formation fractions (not rates) for various different SSPs expanded from figure 6 for clarity. It is important to note that these are the fractions of total mass formed over the lifetime of the galaxy, and not the fractions of light contributing to the recovered spectrum. The light from the youngest populations is some 300x brighter than the oldest

this change. Even ignoring this change in the normalization of the SFR it is clear that the trend for a low redshift peak is no longer present - the SFR appears to fall monotonically to the present day. This interpretation does not exclude a peak at a higher redshift than our eldest bin.

#### 4.5 Stellar population models

Figs. 6c and 7 show the comparison between five different stellar population synthesis models: the Jimenez et al. (2004) SPEED models, the Fioc & Rocca-Volmerange (1997) PEGASE models, the Maraston (2005) RHB models; the Bruzual & Charlot (1993) models and the more modern  $3\text{\AA}$  Bruzual & Charlot (2003) GALAXEV models rebinned to  $20\text{\AA}$ . The comparison is done at  $20\text{\AA}$  for the Salpeter IMF and for the one-parameter dust model. It is important to establish that this analysis cannot say which model set is ‘right’, only assist in understanding the differences between models. The overall shape of the SF is in reasonable agreement - although there are certainly discrepancies between the populations that are recovered. For the very oldest populations the different models agree very well. This is not entirely unexpected of course, as the stars which contribute to this area of the age-metallicity parameter space are well studied and dominate the emission at red wavelengths. The different models also predict roughly similar proportions of the very youngest populations, which rely on similar prescriptions for the evolution of blue massive stars and can be constrained through the emission at the bluest wavelengths. At in-

termediate ages the agreement is not so good: this is likely to be caused, at least in part, by the difficulty in recovering the fraction of intermediate-age stars in stellar populations with declining star formation histories (see discussion by Mathis et al. (2006)). This tends to produce an artificial step around 1 Gyr in the star formation history, except perhaps in the Maraston (2005) model. The different behavior of this model probably results from the different prescription for bright Thermally Pulsing Asymptotic Giant Branch (TP-AGB) stars. The contribution by these stars to the integrated light is still subject to controversy in current population synthesis models. Since our spectra are fitted in addition, any poorly fit component will be replaced by another.

Fig. 8c shows the difference that the various models make to the recovered SFR. It is clear that there is a large spread - as discussed earlier, this is due to the fact that the models contribute both to the estimation of the SFH and the  $V_{\text{max}}$  weights attributed to the galaxies. In all models except those of the PEGASE group the SFR decreases monotonically from the oldest to the youngest bins.

#### 4.6 The impact of resolution, $20\text{\AA}$ vs $3\text{\AA}$

Fig. 6d shows the impact of increasing the spectral resolution of the data. In this case we use the BC03 at resolutions of  $20\text{\AA}$  and  $3\text{\AA}$  on DR3. The differences between the two curves are very small. The maximum deviation is only of about 30% in bin 4 and smaller in bin 5. For the other bins the agreement is remarkable. What this comparison is telling us is that  $20\text{\AA}$  is sufficient resolution to deter-

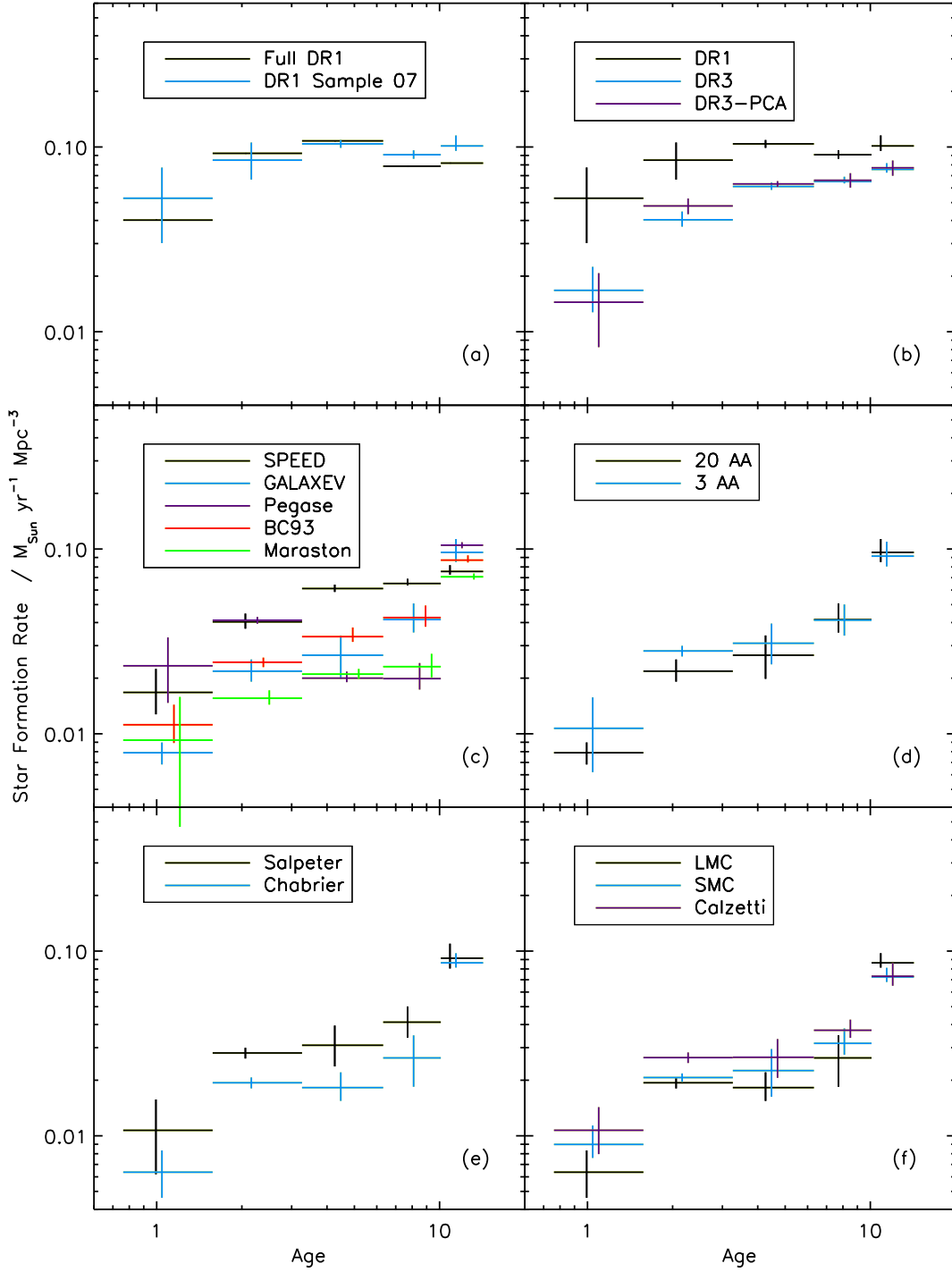


**Figure 8.** The systematic changes in the overall SFR for various modelling choices. The labels show the various modelling choices applied to generate the SFRs,  $V_{max}$ , mass and SFR and are expanded upon in the text. We plot only those bins used for the analysis in the main section, and caution that due to the large  $V_{max}$  corrections there are insufficient galaxies in this sub-sample to draw robust conclusions

mine the average properties of galaxies. The higher resolution does not add much extra information to this. More importantly, the result is not biased at the lower resolution. This is not entirely surprising since the continuum certainly contains information about both age and metallicity of a stellar population (e.g. Jimenez et al. (2004)). The shape of the SFR recovered in Fig. 8d is remarkably consistent between the two resolutions, with a significant variation in only one bin.

#### 4.7 IMF: Salpeter vs. Chabrier.

Fig. 6e and 8e show the impact of changing the initial mass function on the recovered SFF and SFR. In this case we have chosen to work with the BC03 models at  $3\text{\AA}$  resolution. The IMF determines the initial distribution of the number of stars as a function of mass. It is therefore not surprising to find changes in the recovered star formation history for dramatic changes in the IMF. The Chabrier and Salpeter IMF are very similar for masses larger than  $1 - 2 M_{\odot}$  (they are both power laws) while they differ considerably at smaller masses: the Salpeter IMF continues being a power law (with index  $-1.35$ ) while the Chabrier IMF deviates containing a much smaller number of small mass stars relative to the Salpeter IMF. As panel 6e shows the main difference occurs at the oldest bin (bin 1), with smaller differences in bins 2 – 4 and virtually no differences for the youngest bins when the bootstrap error bars are taken into account. This effect is propagated through the  $V_{\text{max}}$  and mass calculation to the SFR. This is more-or-less what one would expect: for the oldest bin, the Chabrier IMF has to compensate its relative lack of low mass stars compared with the Salpeter IMF by forming more of them. The differences then disappear as more massive stars are more dominant at recent ages. It is interesting that although our results will be affected by varying the IMF, it will be in a different sense from the results from instantaneous SFRs attained at high redshift. Where as virtually all instantaneous indicators estimate the total mass of stars from the very high mass UV emitting stars, our technique uses the low mass remnants. The fact that the two approaches agree suggests that the IMFs currently in vogue are along the right lines, and a direct comparison of sufficiently accurate indicators from both the instantaneous and fossil approach could allow IMF fine-tuning. This approach would also require an accurate understanding of the dust in star forming regions, a subject of some controversy in the literature. This topic will be discussed in a future paper.

#### 4.8 Dust modelling

One of the most difficult problems in modelling stellar populations is how to model the attenuation of the population by dust. For our previous study (Heavens et al. 2004) we adopted a simplified model with only one parameter (the attenuation) while the spectral dependence of the attenuation was taken to be that of the Large Magellanic Cloud. Alternate formalisations for the screen are based on the Small Magellanic Cloud, or estimated for starburst galaxies by Calzetti (1997). On the other hand, Charlot & Fall (2000) have proposed that a more accurate modelling of the effects of dust attenuation in galaxies can be achieved by a two-parameter model. In this model one parameter accounts for dust in the giant molecular clouds surrounding young stars (of ages  $< 10$  Myr) and the other parameter the dust in the diffuse ISM. The combination of the two parameters allows a more complex extinction curve to be generated. Unfortunately, since our method does not include the contribution

to the spectrum from emission lines, it is not possible to determine the extinction from the birth cloud from continuum alone.

Fig. 6f and 8f show the differences between the LMC, SMC and Calzetti models for the BC03 models at  $3\text{\AA}$  resolution. The most significant difference occurs clearly at about 0.1 Gyr.

## 5 RESIDUALS OF BEST FIT MODELS

The average residuals from the best-fit solutions of the different models is shown in Fig. 9. This provides a more detailed look at how well the models are faring at reproducing the features in the observed spectra and if some models do better than others. It can be seen that the  $20\text{\AA}$  models cover essentially the same range of spectral features, and it would be impossible to say that one is better than another. The picture changes when we consider the  $3\text{\AA}$  models however, they are clearly superior at minimizing the residuals - even when rebinned to  $20\text{\AA}$  resolution. Although there are still several regions where features are not quite correct, it is on the level of individual lines rather than wide bands of the spectrum. Comparing panels (a) and (b) allows us to investigate the effect of the improvement in photometric calibration between DR1 and DR2-3 on line strengths - practically none, as it should be.

This average deviation should not be confused with average goodness of fit however, as inspection of the relevant average  $\chi^2$  of the samples shows a slightly different story. The models have essentially infinite precision, so there is no penalty associated with rebinning. The converse is true for the spectra, as binning pixels while correctly propagating the error will reduce the standard deviation.

## 6 CONCLUSIONS

We have used MOPED to probe the fossil record of star formation encoded in the spectra of more than 300,000 SDSS-DR3 galaxies to determine stellar populations, metallicity evolution and dust content. We have also investigated the impact of systematics on recovering physical information from the fossil record. Our main conclusions are:

- The main impacts on systematic variation in the estimation of SFR from the fossil record are due to the stellar population model, the calibration of the observed spectra and the choice of the IMF.
- We find strong evidence for downsizing, independent of model choice.
- The overall star formation history of galaxies recovered from the fossil record agrees well with instantaneous formation measurements.
- The mass build-up recovered from our analysis is in good agreement with that predicted from both high redshift studies and the semi-analytic simulations of galaxy formation based on Millennium Run.
- We have identified the cause of many of the residuals from the spectral fits. Stellar population models that provide extra freedom in terms of alpha enhancement should provide better fits.

The fossil record continues to provide a useful tool to unveil the physical conditions of galaxies in the present and the past. With improved models that incorporate alpha-enhancement it should be possible to constrain further models of galaxy formation and evolution and the initial mass function of galaxies.

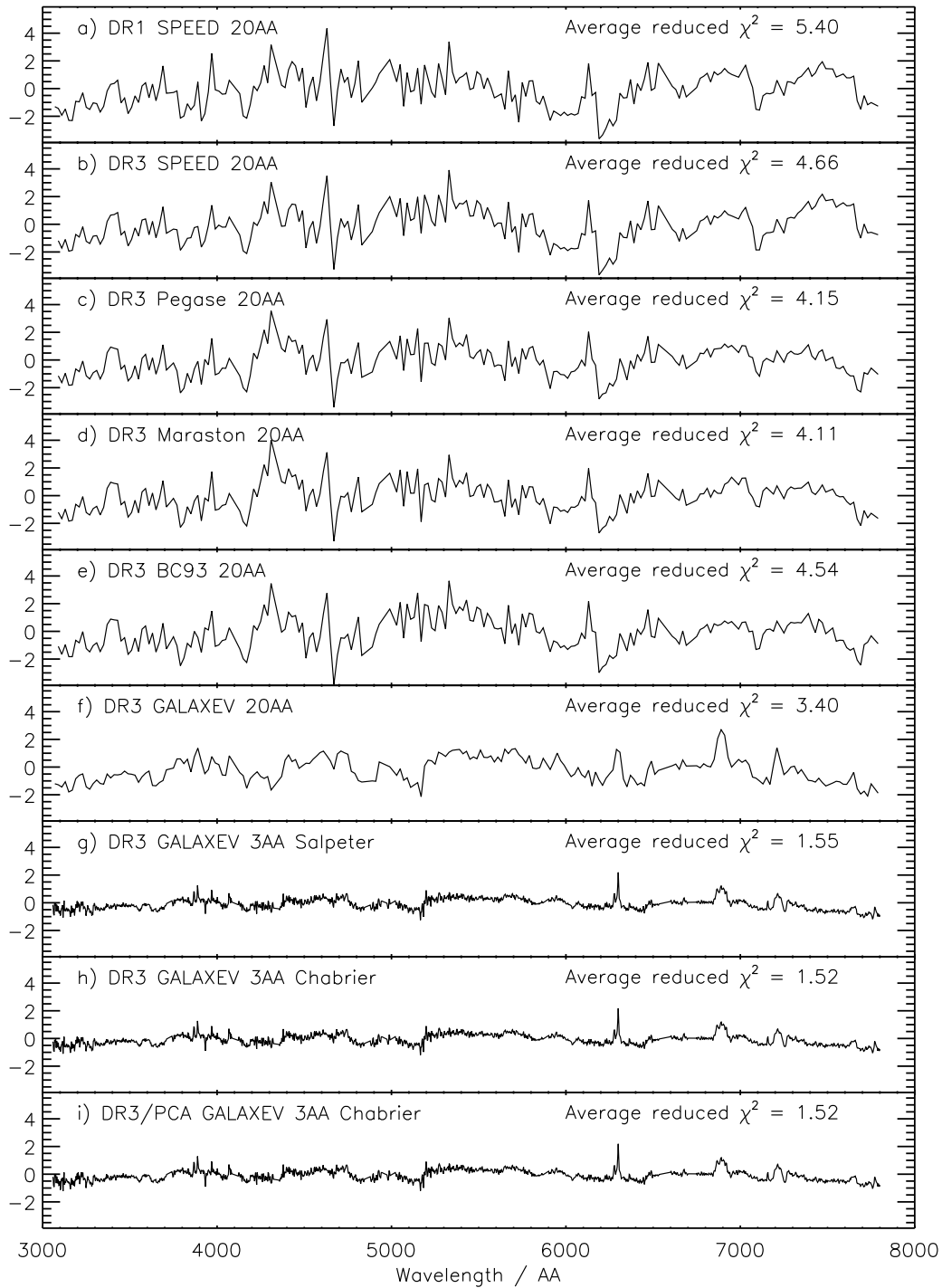


**Figure 9.** Average residuals, following the method used to prepare figure 5 but instead using all the MGS spectra in the two plates. The individual panels are labelled with the models and datasets which were used to generate them. From top to bottom, a) DR1 data, Jimenez et al. (2004) SPEED models; b) DR3 data, SPEED models; c) DR3 data, Fioc & Rocca-Volmerange (1997) PEGASE models; d) DR3 data, Maraston (2005) RHB models; e) Bruzual & Charlot (1993) models; f) DR3 data, Bruzual & Charlot (2003) GALAXEV models rebinned to 20Å; g) DR3 data, GALAXEV models at 3Å resolution using a Salpeter (1955) IMF; h) DR3 data, GALAXEV models at 3Å using a Chabrier (2003) IMF; i) DR3 data cleaned using the skyline extraction method of Wild & Hewett (2005). Residuals are averaged in the rest frame.

**ACKNOWLEDGMENTS**

We thank the anonymous referee for several suggestions which have considerably increased the scope and clarity of the paper.

BP and SC thank the Alexander von Humboldt Foundation, the Federal Ministry of Education and Research, and the Programme for Investment in the Future (ZIP) of the German Government for funding through a Sofja Kovalevskaja award. The research of RJ is partially supported by NSF grants AST-0408698, PIRE-0507768 and NASA grant NNG05GG01G.

BP wishes to thank Paul Hewett for considerable assistance identifying the source of various residuals in Fig. 5.

We acknowledge use of the public IDL routines of Craig Mackwardt, David Fanning and the SDSS idlutils package, and the private SDSS/Milky Way dust compensation routine of Rita Tojeiro. Much of the exploratory work that led to the results contained in this paper benefited from an SQL database created with Gerard Lemson as part of the GAVO project. We wish to thank Darren Croton for providing the data used for comparison with the Millenium Simulation in Figure 1 in electronic form.

Funding for the creation and distribution of the SDSS Archive has been provided by the Alfred P. Sloan Foundation, the Participating Institutions, the National Aeronautics and Space Administration, the National Science Foundation, the U.S. Department of Energy, the Japanese Monbukagakusho, and the Max Planck Society. The SDSS Web site is <http://www.sdss.org/>.

The SDSS is managed by the Astrophysical Research Consortium (ARC) for the Participating Institutions. The Participating Institutions are The University of Chicago, Fermilab, the Institute for Advanced Study, the Japan Participation Group, The Johns Hopkins University, Los Alamos National Laboratory, the Max-Planck-Institute for Astronomy (MPIA), the Max-Planck-Institute for Astrophysics (MPA), New Mexico State University, University of Pittsburgh, Princeton University, the United States Naval Observatory and the University of Washington.

**REFERENCES**

- Abazajian et al. K., 2003, *AJ*, 126, 2081  
 Abazajian et al. K., 2004, *AJ*, 128, 502  
 Abazajian et al. K., 2005, *AJ*, 129, 1755  
 Barger, A. J., Cowie, L. L., Richards, E. A. 2000, *AJ*, 119, 2092  
 Bell, E.F., McIntosh, D.H., Katz, N., Weinberg, M.D., *ApJ*, 2003, 585, 117-120  
 Bell E. F., de Jong R. S., 2001, *ApJ*, 550, 212  
 Borch A., et al., 2006, *A&A*, 453, 869  
 Brinchmann J., Ellis R. S., 2000, *ApJ*, 536, L77  
 Brinchmann J., Charlot S., White S. D. M., Tremonti C., Kauffmann G., Heckman T., Brinkmann J., 2004, *MNRAS*, 351, 1151  
 Bruzual A. G., Charlot S., 1993, *ApJ*, 405, 538  
 Bruzual G., Charlot S., 2003, *MNRAS*, 344, 1000  
 Calzetti D., 1997, *AJ*, 113, 162  
 Chabrier G., 2003, *PASP*, 115, 763  
 Cid Fernandes, R., Mateus, A., Sodré, L., Stasińska, G., & Gomes, J. M. 2005, *MNRAS*, 358, 363  
 Charlot S., Fall S. M., 2000, *apj*, 539, 718  
 Cole, S., et al. 2001, *MNRAS*, 326, 255  
 Condon, J. J., Cotton, W. D., Broderick, J. J. 2002, *AJ*, 124, 675  
 Condon, J. J. 1989, *ApJ*, 338, 13  
 Connolly, A. J., Szalay, A. S., Dickinson, M., SubbaRao, M. U., Brunner, R. J. 1997, *ApJ*, 486, L11  
 Cowie, L. L., Songaila, A., Barger, A. J. 1999, *AJ*, 118, 603  
 Croton D. J., et al., 2006, *MNRAS*, 365, 11  
 Davis et al. M., 2003, in Guhathakurta P., ed., *Discoveries and Research Prospects from 6- to 10-Meter-Class Telescopes II*. Edited by Guhathakurta, Puragra. *Proceedings of the SPIE*, Volume 4834, pp. 161-172 (2003). *Science Objectives and Early Results of the DEEP2 Redshift Survey*. pp 161–172  
 Dickinson M., Papovich C., Ferguson H. C., Budavári T., 2003, *ApJ*, 587, 25  
 Drory N., Salvato M., Gabasch A., Bender R., Hopp U., Feulner G., Pannella M., 2005, *ApJ*, 619, L131  
 Fioc M., Rocca-Volmerange B., 1997, *A&A*, 326, 950  
 Flores, H., et al. 1999, *ApJ*, 517, 148  
 Fontana A., et al., 2004, *A&A*, 424, 23  
 Fukugita, M., Hogan, C.J., Peebles, P.J.E., 1998, *ApJ*, 503, 518  
 Gallego, J., Zamorano, J., Aragón-Salamanca, A., Rego, M. 1995, *ApJ*, 455, L1  
 Gallego, J., García-Dabó, C. E., Zamorano, J., Aragón-Salamanca, A., Rego, M. 2002, *ApJ*, 570, L1  
 Georgakakis, A., Hopkins, A. M., Sullivan, M., Afonso, J., Georgantopoulos, I., Mobasher, B., Cram, L. 2003, *MNRAS*, 345, 939  
 Giavalisco, M., et al. 2004, *ApJ*, 600, L103  
 Glazebrook, K., Blake, C., Economou, F., Lilly, S., Colless, M. 1999, *MNRAS*, 306, 843  
 Glazebrook, K., Baldry, I. K., Blanton, M. R., Brinkmann, J., Connolly, A., Csabai, I., Fukugita, M., Ivezić, Z., Loveday, J., Meiksin, A., Nichol, R., Peng, E., Schneider, D. P., SubbaRao, M., Tremonti, C., York, D. G., 2003, *ApJ*, 587, 55  
 Gordon, K. D., Clayton, G. C., Misselt, K. A., Landolt, A. U., Wolff, M. J., 2003, *ApJ*, 594, 279  
 Gunn et al. J. E., 1998, *AJ*, 116, 3040  
 Haarsma, D. B., Partridge, R. B., Windhorst, R. A., Richards, E. A. 2000, *ApJ*, 544, 641  
 Hammer, F., et al. 1997, *ApJ*, 481, 49  
 Heavens A., Panter B., Jimenez R., Dunlop J. S., 2004, *Nature*  
 Heavens A. F., Jimenez R., Lahav O., 2000, *MNRAS*, 317, 965  
 Hogg, D. W., Cohen, J. G., Blandford, R., Pahre, M. A. 1998, *ApJ*, 504, 622  
 Hopkins, A. M., Connolly, A. J., Szalay, A. S. 2000, *AJ*, 120, 2843  
 Hopkins A. M., 2004, *ApJ*, 615, 209  
 Hughes, D. H., et al. 1998, *Nature*, 394, 241  
 Jimenez R., Flynn C., MacDonald J., Gibson B. K., 2003, *Sci*, 299, 1552  
 Jimenez R., MacDonald J., Dunlop J. S., Padoan P., Peacock J. A., 2004, *MNRAS*, 349, 240  
 Kauffmann G., White S. D. M., Heckman T. M., Menard B., Brinchmann J., Charlot S., Tremonti C., Brinkmann J., 2004, *astro-ph/0402030*  
 Kochanek, C.S., et al. 2001, *ApJ*, 560, 566  
 Lilly, S. J., Le Fèvre, O., Hammer, F., Crampton, D. 1996, *ApJ*, 460, L1  
 Machalski, J., Godlowski, W. 2000, *A&A*, 360, 463  
 Madau, P., Ferguson, H. C., Dickinson, M. E., Giavalisco, M., Steidel, C. C., Fruchter, A. 1996, *MNRAS*, 283, 1388  
 Maraston C., 2005, *MNRAS*, 362, 799  
 Massarotti, M., Iovino, A., Buzzoni, A. 2001, *ApJ*, 559, L105  
 Mathis H., Charlot S., Brinchmann J., 2006, *MNRAS*, 365, 385  
 Moorwood, A. F. M., van der Werf, P. P., Cuby, J. G., Oliva, E. 2000, *A&A*, 362, 9  
 Ocvirk P., Pichon C., Lançon A., Thiébaud E., 2006, *MNRAS*, 365, 46



- Panter B., Heavens A. F., Jimenez R., 2003, MNRAS, 343, 1145
- Panter B., Heavens A. F., Jimenez R., 2004, MNRAS, 355, 764
- Panter B., Thesis, 2005. Available at from the Edinburgh Research Archive at <http://hdl.handle.net/1842/774>
- Persic, M., Salucci, P., 1992, MNRAS, 258, 14
- Pettini, M., Kellogg, M., Steidel, C. C., Dickinson, M., Adelberger, K. L., Giavalisco, M. 1998, ApJ, 508, 539
- Pérez-González, P. G., Zamorano, J., Gallego, J., Aragón-Salamanca, A., Gil de Paz, A. 2003, ApJ, 591, 827
- Rudnick G. H., Rix H.-W., Franx M., Labbe I., FIRES Collaboration, 2003, AAS, 36, 591
- Sadler, E. M., et al. 2002, MNRAS, 329, 227
- Salpeter E. E., 1955, ApJ, 121, 161
- Salucci, P., Persic, M., 1992, MNRAS, 309, 923
- Schechter, P. 1976, ApJ, 203, 297
- Serjeant, S., Gruppioni, C., Oliver, S. 2002, MNRAS, 330, 621
- Shen S., Mo H. J., White S. D. M., Blanton M. R., Kauffmann G., Voges W., Brinkmann J., Csabai I., 2003, MNRAS, 343, 978
- Spergel D. N., Verde L., Peiris H. V., Komatsu E., Nolte M. R., Bennett C. L., Halpern M., Hinshaw G., Jarosik N., Kogut A., Limon M., Meyer S. S., Page L., Tucker G. S., Weiland J. L., Wollack E., Wright E. L., 2003, ApJS, 148, 175
- Steidel, C. C., Adelberger, K. L., Giavalisco, M., Dickinson, M., Pettini, M. 1999, ApJ, 519, 1
- Stoughton et al. C., 2002, AJ, 123, 485
- Strauss et al. M. A., 2002, AJ, 124, 1810
- Sullivan, M., Treyer, M. A., Ellis, R. S., Bridges, T. J., Milliard, B., Donas, J., 2000, MNRAS, 312, 442
- Sullivan, M., Mobasher, B., Chan, B., Cram, L., Ellis, R., Treyer, M., Hopkins, A. 2001, ApJ, 558, 72
- Teplitz, H. I., Collins, N. R., Gardner, J. P., Hill, R. S., Rhodes, J. 2003, ApJ, 589, 704
- Thomas D., Maraston C., Bender R., 2003, MNRAS, 339, 897
- Thomas, D., Maraston, C., Bender, R., & Mendes de Oliveira, C. 2005, ApJ, 621, 673
- Tremonti C. A., Heckman T. M., Kauffmann G., Brinchmann J., Charlot S., White S. D. M., Seibert M., Peng E. W., Schlegel D. J., Uomoto A., Fukugita M., Brinkmann J., 2004, ApJ, 613, 898
- Tresse, L., Maddox, S. J., Le Fèvre, O., Cuby, J.-G. 2002, MNRAS, 337, 369
- Tresse, L., Maddox, S. J. 1998, ApJ, 495, 691
- Treyer, M. A., Ellis, R. S., Milliard, B., Donas, J., Bridges, T. J. 1998, MNRAS, 300, 303
- Wild V., Hewett P. C., 2005, MNRAS, 358, 1083
- Wilson, G., Cowie, L. L., Barger, A., Burke, D. J. 2002, AJ, 124, 1258
- Yan, L., McCarthy, P. J., Freudling, W., Teplitz, H. I., Malumuth, E. M., Weymann, R. J., Malkan, M. A. 1999, ApJL, 519, L47
- York et al. D., 2000, AJ, 120, 1579

